Chinese Journal of
POLYMER SCIENCE

RESEARCH ARTICLE

https://doi.org/10.1007/s10118-025-3520-6
Chinese J. Polym. Sci. **2026**, *44*, 803–812

Multifunctional CNT/cellulose-BN/PVA Composites Integrating Dual-continuous Network Structure with Gradient Conductivity for Electromagnetic Interference Shielding and Joule Heating

Xiao-Rui Wang[a,†], Ting-Ting Liu[b,†], Cheng-Hua Cui[c], Xin Xu[d], and Liang-Qing Zhang[a*]

[a] *College of Materials Science and Engineering, Xi'an University of Science and Technology, Xi'an 710054, China*
[b] *Department of Pediatrics, Northwest Women's and Children's Hospital, Xi'an 710061, China*
[c] *Zhejiang Engineering Research Center for Interface Technology of Medical Polymers and Devices, Shaoxing Key Laboratory of Healthcare Materials and Application Technology, and Center for Healthcare Materials, Shaoxing Institute, Zhejiang University, Shaoxing 312099, China*
[d] *Zhejiang Tongzheng Pipeline Technology Co., LTD., Zhejiang 312030, China*

Electronic Supplementary Information

Abstract In this study, an architecture featuring a gradient conductive network structure and three-dimensional dual-continuous network structure is constructed in a carbon nanotubes/cellulose-boron nitride/poly(vinyl alcohol) (CNT/cellulose-BN/PVA) composite. Using cellulose aerogel as a template, CNT were incorporated into the cellulose template by vertically impregnating the CNT suspension. Following the impregnation of BN/PVA and high-pressure compression, three-dimensional dual-continuous network structure was successfully constructed in the CNT/cellulose-BN/PVA composite. The comprehensive performance of the composite, including electromagnetic interference (EMI) shielding and Joule heating performance, was investigated. The results indicate that the total EMI shielding effectiveness (SE) for the CNT/cellulose-BN/PVA composite reveals similar values for electromagnetic waves incident from different directions, but totally different shielding mechanisms. For the CNT/cellulose-BN/PVA composite with three impregnation cycles of CNT, the EMI SE values exceeded 39 dB for electromagnetic waves incident from both the high- and low-CNT-content sides. 93% of the microwaves were reflected when electromagnetic waves were incident from the high-CNT-content side, while the reflection coefficient decreased to 0.44 for the transverse direction. In addition, the construction of the dual-continuous network structure enabled the composite to exhibit both excellent electrical conductivity and good thermal conductivity simultaneously, endowing the material with good Joule heating performance. CNT/cellulose-BN/PVA composite films have significant potential for application as EMI shielding materials in extremely cold weather.

Keywords Cellulose; Dual-continuous network structure; Gradient conductivity; Electromagnetic interference shielding; Joule heating

Citation: Wang, X. R.; Liu, T. T.; Cui, C. H.; Xu, X.; Zhang, L. Q. Multifunctional CNT/cellulose-BN/PVA composites integrating dual-continuous network structure with gradient conductivity for electromagnetic interference shielding and joule heating. *Chinese J. Polym. Sci.* **2026**, *44*, 803–812.

INTRODUCTION

In the booming 5G communication technology and Internet era, electronic products are almost always accompanied by people's entire life cycle. Electromagnetic waves bring great convenience to people but also lead to unwelcome electromagnetic pollution and information leakage.[1–3] Therefore, the development of high-performance electromagnetic interference (EMI) shielding materials is of great significance for protecting electronic equipment against interference and human health.[4–6]

Traditional EMI shielding materials are mostly metal materials with high conductivity,[7] and such materials have the characteristics of high density, high rigidity, easy oxidation, and easy corrosion, which severely limit their application fields.[8–10] Compared with traditional metal materials, polymer-based EMI shielding composites have been developed rapidly in the field of electromagnetic protection owing to their advantages, such as light weight, easy processing, and strong designability.[11,12]

To achieve satisfactory EMI shielding effectiveness (SE) in polymer composites, the construction of a three-dimensional (3D) conductive network structure is very effective.[13–15] Guo *et al.*[16] constructed a polyimide/boron nitride (BN) nanosheet/$Ti_3C_2T_x$ MXene composite film with a 3D conductive network; the EMI SE reached 49.2 dB. Lu *et al.*[17] developed an isolated conductive network structure in a multi-wall carbon nanotube (CNT)/cellulose composite. The composite exhibited an EMI SE as high as 49.2 dB. Acrylonitrile-butadiene-styrene-based composite foams were fabricated by Wang *et al.*,[18] exhibiting an EMI SE as high as 73.5 dB. On the

* Corresponding author, E-mail: liangqingzhang@xust.edu.cn
† These authors contributed equally to this work.
Received August 23, 2025; Accepted November 28, 2025; Published online February 6, 2026

one hand, the construction of the 3D conductive network structure can effectively increase the conductivity, leading to a satisfying total EMI SE. On the other hand, high conductivity will inevitably increase the impedance mismatch between the material surface and the air, resulting in increased reflection when the electromagnetic waves reach the surface of the material, causing serious secondary electromagnetic radiation pollution.[19,20] Therefore, the development of a composite with simultaneously high EMI SE and absorption coefficient (*A*) for electromagnetic waves has become a research hotspot.[7]

The preparation of EMI shielding materials with non-uniform conductive structures is a highly promising strategy to address the contradiction between EMI SE and *A* in a uniform substance. By controlling the upper and bottom surfaces with different conductivities, Luo *et al*.[21] revealed the anisotropic EMI shielding performance of Janus multi-walled CNT/cellulose nanofibers/poly(3,4-ethylenedioxythiophene):polystyrene sulfonate composite film, achieving an improved *A* and EMI SE as high as 61 dB. Lei *et al*.[22] prepared silver fractal dendrite/thermoplastic polyurethane composite foams with a gradient conductive structure through layer-by-layer construction, which presented an excellent EMI SE of 88.5 dB and an ultra-low electromagnetic microwave reflection shielding effectiveness (SE_R) of 0.29 dB. The simultaneous high EMI SE and low reflection originate from the unique electromagnetic wave dissipation path of "low reflection-absorption-high reflection-reabsorption". Xu *et al*.[23] constructed a gradient shielding layer with a reflection coefficient (*R*) of 0.39 and an excellent EMI SE (87.2 dB) by depositing magnetic iron/iron oxide on reduced graphene oxide (rGO@Fe_3O_4) and a silver-coated tetraneedle. The construction of a gradient conductive structure is an effective strategy for achieving high EMI SE while maintaining low reflection characteristics.[24,25]

In addition to the superior EMI shielding performance, good comprehensive performance is required, considering the practical application of EMI shielding materials. For example, many large outdoor equipment systems require measures to mitigate the impact of extreme weather conditions on their EMI shielding performance,[26] which requires materials with good EMI shielding and Joule heating performance. To obtain better Joule heating performance, the material must have good electrical and thermal conductivities at the same time. The construction of a 3D conductive structure can endow the composite with good electrical conductivity. However, owing to the interfacial thermal resistance between the 3D network structure and matrix, the thermal conductivity is often poor, resulting in a longer Joule heating process time and uneven temperature distribution. Therefore, the construction of an effective thermal conductive path and the reduction of the interfacial thermal resistance are key to improving the comprehensive performance of the material. Taking this into consideration, the architecture of a thermal/electrical dual-continuous network structure, which can provide multiple reflection interfaces for electromagnetic waves while minimizing the interfacial thermal resistance, seems to be an effective strategy for solving the current problem.[27,28]

In this study, cellulose aerogel was utilized as a template, and a gradient conductive 3D network structure was constructed within the material by vertically impregnating a CNT suspension. After subsequent BN/poly(vinyl alcohol) (PVA) impregnation-hot pressing molding, the CNT/cellulose-BN/PVA dual-continuous network structure was successfully constructed. The obtained CNT/cellulose-BN/PVA composite exhibited excellent EMI shielding, thermal conductivity, and Joule heating. This provides a solid foundation for its use in the construction of EMI shielding materials for applications in extremely cold weather conditions.

EXPERIMENTAL

Materials

Cotton linters with a degree of polymerization (DP) of 500±50 were supplied by Hubei Jinhuan Ltd. (China). Multi-wall CNT with a diameter of 5–15 nm and a length of 0.5–2 μm were provided by Jiangsu Xianfeng Nanomaterials Technology Co., Ltd. (China). Analytical grade urea, NaOH, cetyltrimethylammonium bromide (CTAB), and tertiary butanol (TBA) (analytical-grade) were obtained from Xi'an Daosheng Chemical Technology Co., Ltd. The PVA sample, which had a molecular weight (MW) ranging from 17600 g·mol^{-1} to 26400 g·mol^{-1}, was obtained from Anhui Wanwei Unit Co., Ltd. (China). Hexagonal BN with an average particle size of 100 nm and 99.9% purity was purchased from Jinan Zhiding Welding Materials, Ltd. (China).

Preparation of Cellulose Aerogel

First, a NaOH/urea/aqueous solution with a mass ratio of 7:12:81 was prepared. This solution was frozen in a refrigerator at −12.5 °C. 2.5 g of cellulose was added to 100 g of the NaOH/urea/aqueous solution and mechanically stirred for 5 min to obtain a cellulose/NaOH/urea/aqueous solution. The solution was centrifuged at 8000 r/min for 5 min, and the resulting solution was poured into a flat-bottom cylindrical mold, and placed in an oven at 70 °C for 72 h to form a hydrogel. Subsequently, the cellulose hydrogel was immersed in water. The water was changed every 2 h until the pH of the water was approximately 7, indicating that NaOH and urea were completely removed. The hydrogel was completely immersed in 10 wt% TBA/water solution for 48 h. Finally, the cellulose hydrogel was first frozen in a refrigerator at −25 °C and then vacuum freeze-dried (−50 °C, 20 Pa) for 48 h to obtain the cellulose aerogel.

Preparation of CNT/Cellulose Composite Aerogel

As shown in Fig. 1, 2.5 g of CNT and CTAB (weight ratio of CNT to CTAB was 1:0.8) were added to 81 g of deionized water and ultrasonically treated for 30 min to prepare the CNT/water suspension. A certain amount of CNT suspension was dripped into a cylindrical mold. The cellulose aerogel was fixed on a sample holder, with the bottom of the cellulose aerogel parallel to the liquid level of the CNT suspension. The cellulose aerogel gradually absorbed the CNT suspension through capillary action. The bottom of the cellulose aerogel was controlled to maintain contact with the CNT suspension until all the CNT suspensions were absorbed into the cellulose aerogel. The samples were frozen at −25 °C for 12 h. After freezing, the samples were placed in a freeze dryer (−50 °C, 20 Pa) for 48 h. The weight content of CNT was calculated by weighing the sample before and after the immersion-drying process. The vertical immersion-drying process was repeated once, twice, and thrice to obtain CNT/cellulose composite aerogels with different CNT contents, which were

https://doi.org/10.1007/s10118-025-3520-6

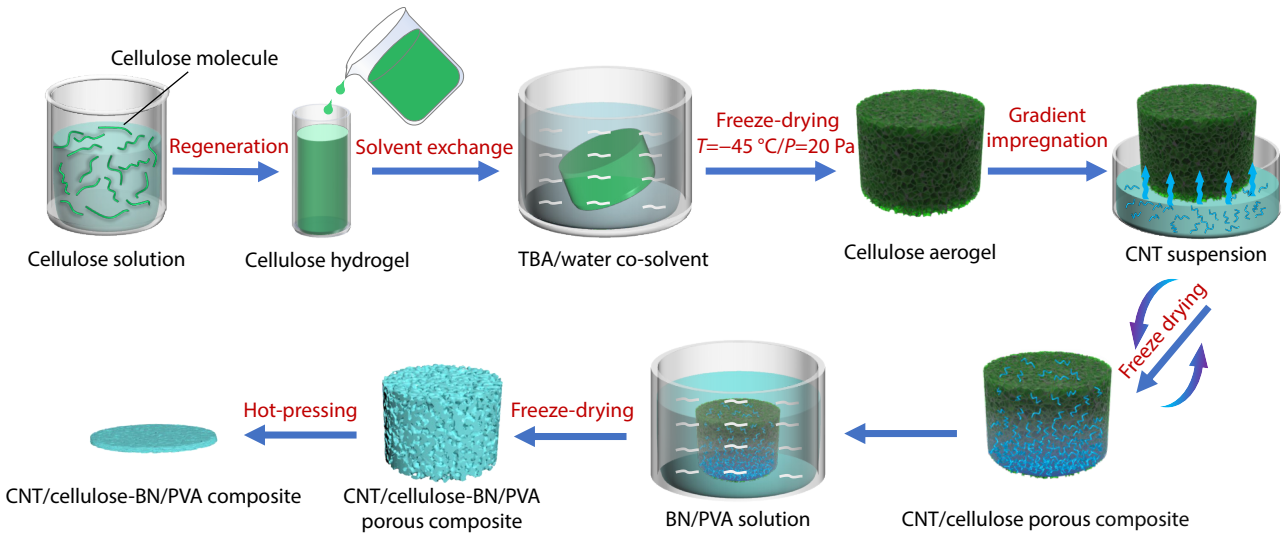

Fig. 1 Schematic illustration of the preparation process of CNT/cellulose-BN/PVA composites.

coded as CNT-*x*, where x represents the "vertical immersion-drying" times.

Preparation of CNT/Cellulose-BN/PVA Composites

As shown in Fig. 1, 0.22 g of BN powder was added to 38 g of deionized water and ultrasonicated for 30 min to obtain the BN suspension. A BN/PVA solution was obtained by adding 2 g of PVA to the BN suspension and magnetic stirring at 80 °C for 30 min. Subsequently, the prepared CNT/cellulose composite aerogel was completely immersed in the BN/PVA solution for 30 min and then frozen at –45 °C for 12 h. Immediately after the freezing process, the samples were vacuum-freeze-dried for 48 h. The samples were weighed before and after the "impregnation-freeze drying" process to obtain the weight content of BN/PVA in the CNT/cellulose-BN/PVA composite. Finally, the sample was hot-pressed at 100 MPa and 100 °C for 5 min to obtain a CNT/cellulose-BN/PVA composite. For simplicity, the CNT/cellulose-BN/PVA composite is denoted as CNT-*x*/BN, where x represents the impregnation time of CNT.

Characterizations

To observe the microstructure of the CNT/cellulose-BN/PVA composites, the samples were examined using scanning electron microscopy (SEM, S-4800, Hitachi, Japan). The samples were immersed in liquid nitrogen for at least 30 min and rapidly quenched to obtain quenched cross sections. The quenched cross-sections were sprayed with gold and observed at an accelerating voltage of 5 kV. To observe the distribution state of CNT in the CNT/cellulose-BN/PVA composite, a piece of CNT/cellulose-BN/PVA composite was embedded in epoxy, and a cross-section (about 800 μm) was obtained using a microtome equipped with a steel knife. De-crossed polarized optical microscopy (dePOM) observations were performed on the cross-sections using an Olympus BX51 microscope (Olympus Co., Japan). The resistivity of the CNT/cellulose-BN/PVA composites was measured using an SDY-6 four-probe tester. Three points were measured for each sample and the average value was calculated. The electrical conductivity was calculated using the formula $\sigma=1/\rho$, where σ (S·m^{-1}) is the electrical conductivity and ρ (Ω·m) is the electrical resistivity. The EMI SE of the CNT/cellulose-BN/PVA composites in the range of 8.2–12.4 GHz (X-band) was characterized using an ASTM ES7-83 coaxial test system. The scattering parameters (S11, S22, S12, and S21) of the samples were obtained by recording their data curves in the frequency range. *R*, *A*, transmission coefficient (*T*), SE_R, electromagnetic microwave absorption shielding effectiveness (SE_A), and total shielding effectiveness (SE_T) were calculated according to Eqs. S(1)–S(6) (in the electronic supplementary information, ESI). The EMI shielding performance was tested when the electromagnetic waves were incident from the high-CNT side and when the electromagnetic waves were incident from the low-CNT side. The diffusion coefficient and specific heat capacity were measured using a laser flash thermal conductivity meter (LFA 467 HyperFlash, NETZSCH, Germany). Each specimen was tested 5 times. Detailed testing and calculation procedures were provided in ESI. The heat-transfer process of the composite was simulated using COMSOL version 6.3. The Joule heating properties of the samples were characterized by infrared thermal imaging (CA73, FLIR, Chauvin Arnoux) at an applied voltage of 1–5 V. The mechanical properties of the samples were determined using a universal tensile instrument (model 5576, Instron Instruments) with a span length of 15 mm and a testing speed of 3 mm/min. Before testing, the composite was cut into rectangular strips approximately 5 mm in width and 20 mm in length.

RESULTS AND DISCUSSION

Microstructures of the CNT/Cellulose-BN/PVA Composites

As shown in Fig. 2(a), the CNT/cellulose composites exhibit a 3D lamellar porous network structure with an average pore size of approximately 200 μm. After the uniform impregnation of BN/PVA and hot pressing, the pore structure disappeared, and the composite exhibited a dense dual-continuous network structure. To observe the distribution of CNT in the CNT-3/BN composite, two parts of the material were selected for magnified observation (Fig. 2b). It is clearly observed that CNT aggregate at the interface of cellulose and PVA, which forms a conductive network structure, and the CNT content in Fig. 2(c_2) is higher than that shown in Fig. 2(c_1), which reflects the gradient

distribution of CNT in the CNT-3/BN composite. A dual-continuous network structure composed of the CNT/cellulose and BN/PVA phases is shown in Fig. 2(d). It is worth noting that the dual-continuous network structure was oriented horizontally, which was ascribed to the horizontal yield of the pore walls during the hot-pressing process. As indicated, the relatively smooth sections correspond to the BN/PVA phase, and the rough areas originate from cellulose and CNT. The interface between the CNT/cellulose and the BN/PVA phase is further observed under higher magnification, as shown in Fig. 2(e). It can be clearly observed that the two phases are closely combined without any cracks, which results from the fact that cellulose has good compatibility with PVA. The distribution of BN in the composites is shown in Fig. 2(f). It is obvious that BN is uniformly distributed in the PVA phase, benefiting from the relatively good compatibility between BN and PVA, as well as the solution mixing method. DePOM observations were performed, as shown in Fig. 3(a). The distribution of CNT in the CNT-3/BN composite can be easily identified because of the light transmittance difference; that is, the CNT-enriched region appears to be dark, the cellulose matrix exhibits higher brightness owing to less visible light absorption and birefringence caused by high crystallinity,[29] and the BN/PVA phase appears to be gray. It is obvious that a horizontally aligned dual-continuous network structure is formed in the CNT/cellulose-BN/PVA composite after compression molding, while CNT are aggregated at the cellulose-PVA interface. The distribution of CNT in the composite exhibits an overall gradient trend along the impregnation direction; that is, bundles of CNT are clustered densely at the bottom and become progressively sparser towards the top of the material. Furthermore, the brightness distribution of the composite quantitatively reflects the gradient distribution of the CNT along the impregnation direction (Fig. 3b).

Electrical Conductivity and EMI Shielding Performance of the CNT/Cellulose-BN/PVA Composites

The SEM results demonstrated that the CNT were gradationally distributed in the CNT/cellulose-BN/PVA composites. Accordingly, the composites were expected to exhibit gradient con-

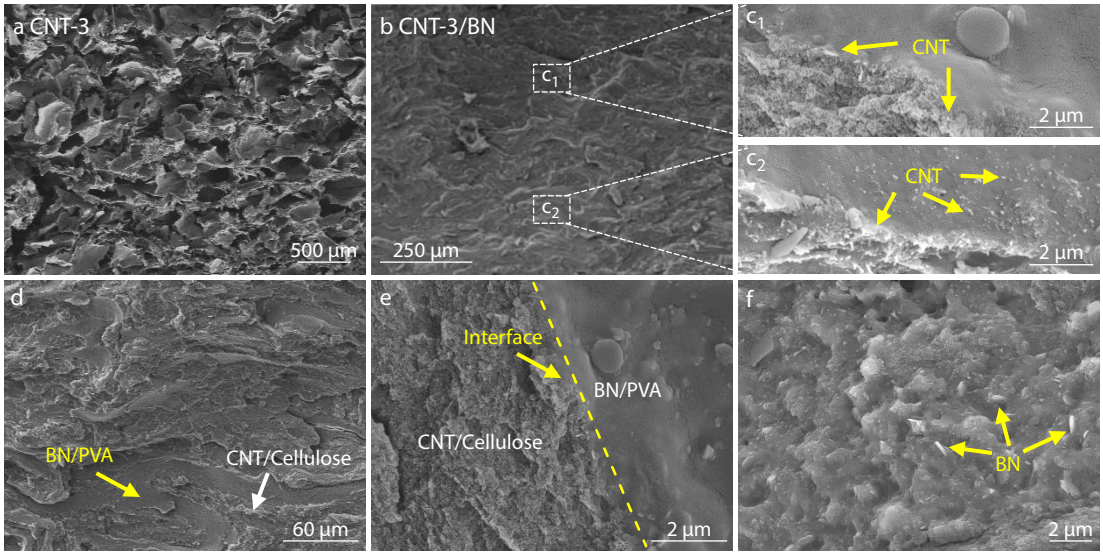

Fig. 2 SEM images of (a) CNT/cellulose porous composite and (b) CNT-3/BN composite, (c_1) and (c_2) are the partial enlargements of sections c_1 and c_2 in Fig. 2(b), (d) dual-continuous network structure, (e) interface between CNT/cellulose and BN/PVA and (f) distribution state of BN in CNT-3/BN composite.

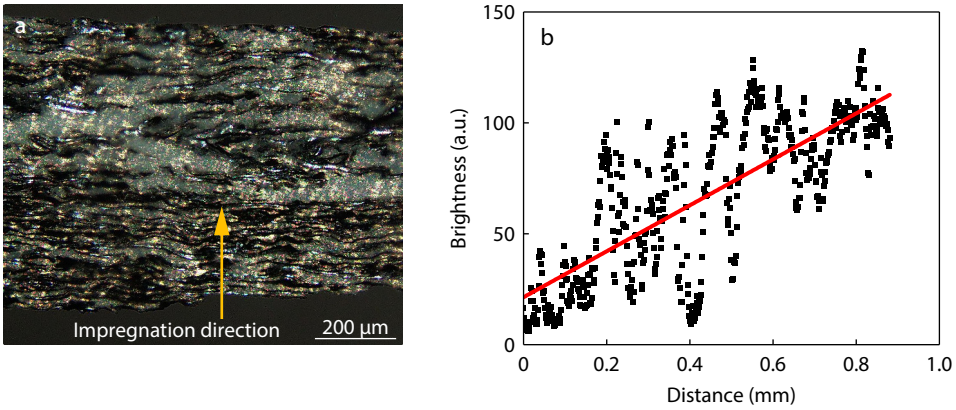

Fig. 3 (a) DePOM image demonstrating the distribution state of CNT in the CNT/cellulose-BN/PVA composite and (b) the brightness distribution along the impregnation direction.

https://doi.org/10.1007/s10118-025-3520-6

ductivities. As shown in Fig. 4(a), all the electrical conductivities of the high-CNT-content side are higher than those of the low-CNT-content side. Take CNT-1/BN as an example, the electrical conductivity for the high-CNT-content side is 23.29 S·m^{-1}, which is 3.93 times higher than that of the low-CNT-content side. In addition, the electrical conductivity increases with increasing impregnation time, which is ascribed to the increase in CNT content (Table S1 in ESI); thus, more CNT nanofillers participate in the construction of the electrically conductive network structure, leading to a higher electrical conductivity. For example, the electrical conductivity of the high-CNT-content side of CNT-1/BN is 23.29 S·m^{-1}. With the increase of impregnation times to 3, the CNT content increases from 3.1 wt% to 9.6 wt%, and the electrical conductivity reaches 109.86 S·m^{-1}. We evaluated the EMI shielding performance of the CNT/cellulose-BN/PVA composites when microwaves were incident from the high CNT content side to the low CNT content side (denoted as high-low) and the transverse direction (denoted as low-high), respectively. From Fig. 4(b), it can be seen that SE_T increases with CNT impregnation time. With only one impregnation, the SE_T reaches 25.2 dB, which exceeded the commercial standard of 20 dB. When the impregnation is increased to three times, the SE_T reaches 39.2 dB, which indicates that 99.98% of the electromagnetic waves are shielded by the material. In addition, the CNT/cellulose-BN/PVA composites presented almost identical EMI SE values for the low-high and high-low transmission directions. Although the composite presents a similar SE_T when microwaves are incident from different directions, the EMI shielding mechanisms are distinctly different. For example, when electromagnetic waves are incident from the high-CNT-content side of the CNT-3/BN composite, the SE_R, SE_A, and SE_T are 12.8, 26.5, and 39.3 dB (Fig. 4c), respectively. When electromagnetic waves are incident from the low-CNT-content side of the CNT-3/BN composite, the SE_R, SE_A, and SE_T are 2.5, 36.6, and 39.2 dB (Fig. 4c), respectively. Although the SE_T are similar, the SE_A is much higher when the electromagnetic waves are incident from the low-CNT-content side, proving that the sample exhibits a higher electromagnetic wave adsorption capacity. As shown in Fig. 4(d), for the CNT-3/BN composite, when the electromagnetic waves are incident from the high-CNT-content side, *R* is as high as 0.93, whereas *A* is only 0.07, demonstrating that most microwaves are reflected. Conversely, when electromagnetic waves are incident from the low-CNT-content side, *R* decreases to 0.44 and *A* increases to 0.56, achieving an absorption-dominated shielding mechanism. This is mainly because the low-CNT-content side has a lower conductivity, so that the material surface has a higher impedance match with the surrounding air,[30,31] which effectively reduces the reflection of electromagnetic waves at the material surface, and incident microwaves are adsorbed by the material. To investigate the absorption mechanism, the electromagnetic parameters of the CNT/cellulose-BN/PVA composites were characterized (Fig. S3 in ESI). First, the ε' values of all the samples are observed to decrease with increasing frequency, which could be attributed to the polarization hysteresis at higher frequencies and typical frequency dispersion. Moreover, both ε' and ε'' of CNT-3/BN are

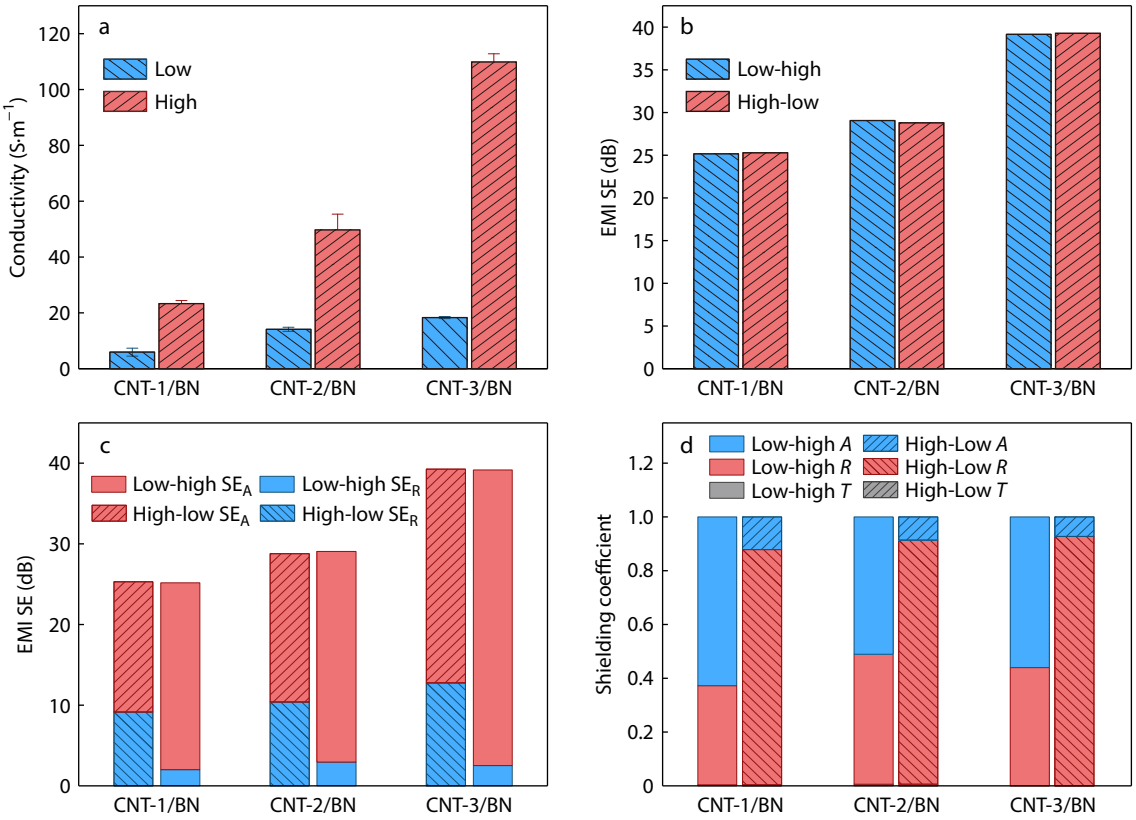

Fig. 4 (a) Conductivity, (b) SE_T, (c) SE_R and SE_A, and (d) shielding coefficients of CNT/cellulose-BN/PVA composites with different CNT filler contents.

https://doi.org/10.1007/s10118-025-3520-6

higher than those of CNT-1/BN. This result is ascribed to the higher CNT content, which collectively contributes to a denser electron transport network, enhancing the dielectric loss.[32] The Cole-Cole plots for both CNT-1/BN and CNT-3/BN display two distinct sections, that is, the linear relationship area in the low-frequency region and the semicircle area in the high-frequency region, which correspond to dielectric loss caused by interface polarization and Debye relaxation polarization, respectively. Furthermore, the relatively high electrical conductivity of the CNT/cellulose-BN/PVA composites plays a significant role in the ohmic loss. Generally, the effects of interfacial polarization, debye polarization, and ohmic loss facilitate the attenuation of microwaves in the material.[33]

EMI Shielding Mechanism of the CNT/Cellulose-BN/PVA Composites

Fig. 5 shows the microwave dissipation process in the gradient CNT/cellulose-BN/PVA composite. When the electromagnetic waves are incident from the low-CNT-content side of the conductive gradient CNT/cellulose-BN/PVA composite (left), the impedance between the material surface and air is well matched. Thus, only a small amount of electromagnetic waves are reflected, and most of them enter the material. With the propagation of microwaves in the material, they are progressively attenuated by ohmic and polarization losses between the dual-continuous network structure, which converts electromagnetic energy into heat. The good electrical conductivity of the CNT plays a significant role in ohmic loss, and this effect is continuously amplified with the increase in CNT content in the CNT/cellulose-BN/PVA composite. The heterogeneous interfaces of CNT/cellulose and CNT/PVA significantly contributed to the interfacial polarization loss. Additionally, the 3D network structure allows multiple reflections of the electromagnetic waves at multiple interfaces in the dual-continuous network structure,[34,35] and the reflection ability of later interfaces continues to increase, forming an absorption-reflection-reabsorption transmission path inside the material. As a result, the electromagnetic waves are trapped in the CNT/cellulose-BN/PVA composite until they are structurally absorbed or attenuated as heat *via* microcurrent and interfacial polarization losses. Upon incidence from the reverse direction (right), that is, from high CNT concentration to low concentration, most of the electromagnetic waves are reflected on the surface of the material owing to the impedance mismatch between the material surface and air,[21,34] resulting in a reflection-based EMI shielding mechanism. The significance of the gradient conductive structure is that it can not only enhance the microwave adsorption ability, but also tune the shielding mechanism by simply altering the incident direction.

Thermal Conductivity and Joule Heating Performance of the CNT/Cellulose-BN/PVA Composites

As can be seen from Fig. 6(a), the thermal conductivity of the composite gradually increases with increasing CNT impregnation time. In addition, relatively lower thermal conductivities along the cross-plane direction are achieved compared to the in-plane direction at high CNT contents. The in-plane and cross-plane thermal conductivities of CNT-1/BN are 0.24 and 0.18 $W \cdot m^{-1} \cdot K^{-1}$, respectively, and the corresponding thermal conductivities of CNT-3/BN increase to 0.27 and 0.54 $W \cdot m^{-1} \cdot K^{-1}$, respectively. This is mainly because, with the increase in the CNT content, a close connection between the CNT was established, forming a horizontally oriented thermal conduction path and providing a fast transmission path for phonons, as schematically illustrated in Fig. 6(a). To elucidate the difference in thermal conductivity between the in-plane and cross-plane directions, the transient heat-transfer processes of the finite-element simulations were analyzed. The model geometry and detailed parameters are provided in Table S2 and Fig. S4 (in ESI). In this analysis, the initial temperature of the system was set to 20 °C, and the bottom (during the cross-plane heat transport process) or left side (during the in-plane heat transport process) of the model was fixed at 80 °C as a thermostatic heat source. The surroundings of the model were thermally insulated, and the heat transfer conditions, such as convection and radiation, were neglected. Fig. 7 shows the temperature distribution in the model over time. It is evident that the heat conduction is faster in the in-plane direction. Owing to the high thermal conductivity of CNT, the heat flow passes rapidly along the horizontally oriented CNT network. In the cross-plane direction, the heat transfer path involves numerous CNT/cellulose and CNT/PVA interfaces. Owing to its high interfacial thermal resistance, the heat trans-

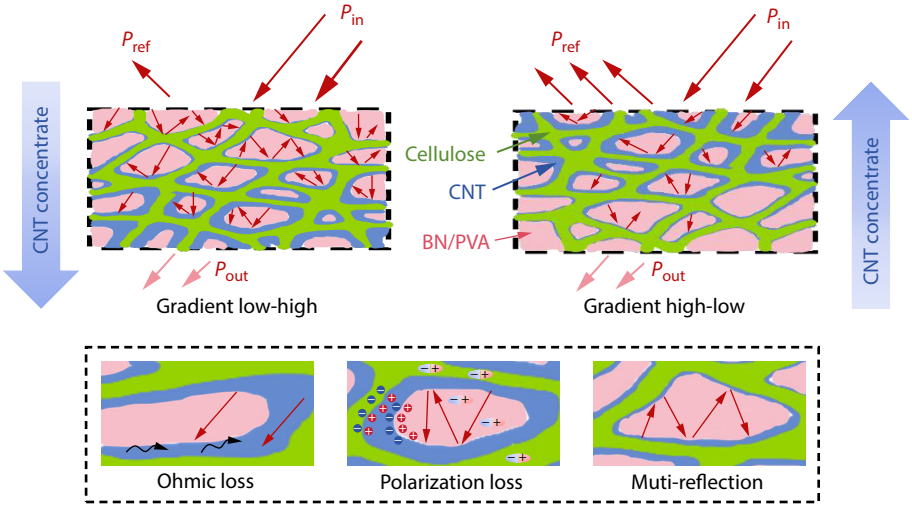

Fig. 5 Schematic illustration of EMI shielding mechanism for CNT/cellulose-BN/PVA composite.

https://doi.org/10.1007/s10118-025-3520-6

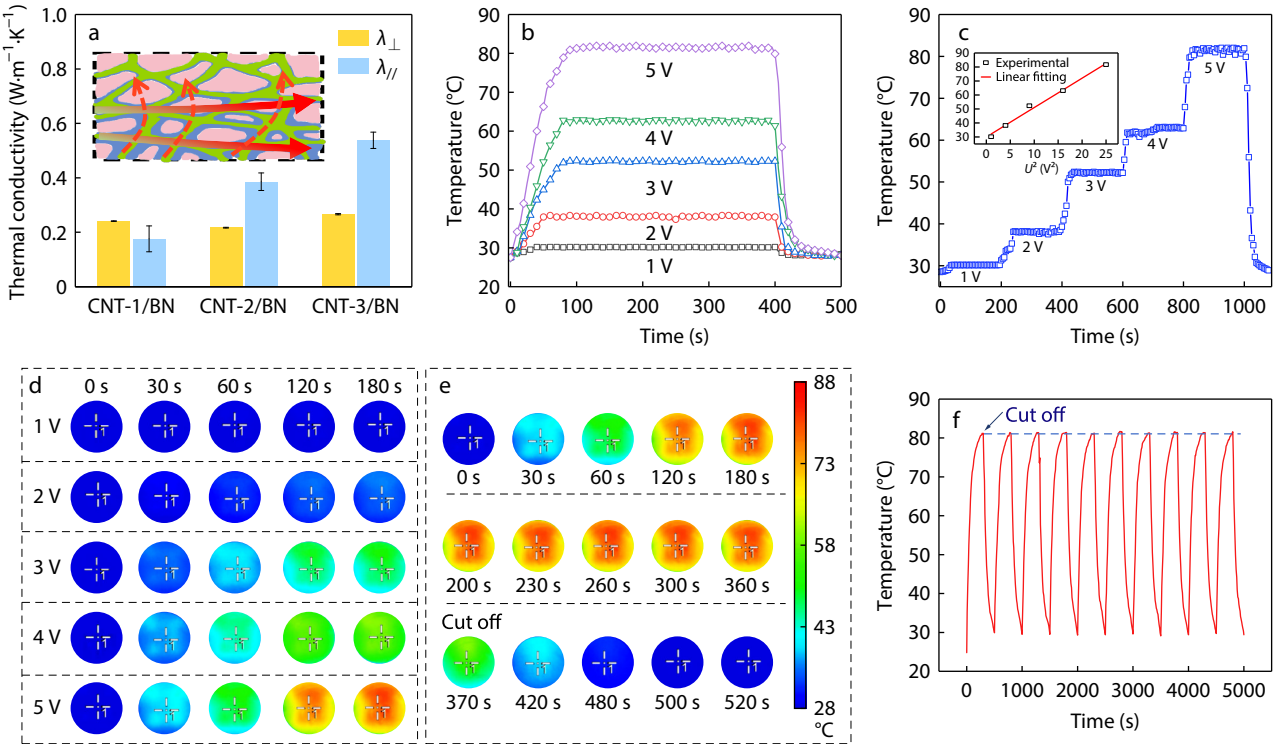

Fig. 6 (a) Thermal conductivity of CNT/cellulose-BN/PVA composites; (b) Time-dependent surface temperatures of the CNT-3/BN composite material at different input voltages; (c) Surface temperatures of the CNT-3/BN composite material with gradient voltage variation; (d) Infrared images of the CNT-3/BN composite material at various input voltages; (e) Infrared images of the CNT-3/BN composite at an input voltage of 5 V and (f) cyclic stability of CNT-3/BN composite material at 5 V for 10 cycles.

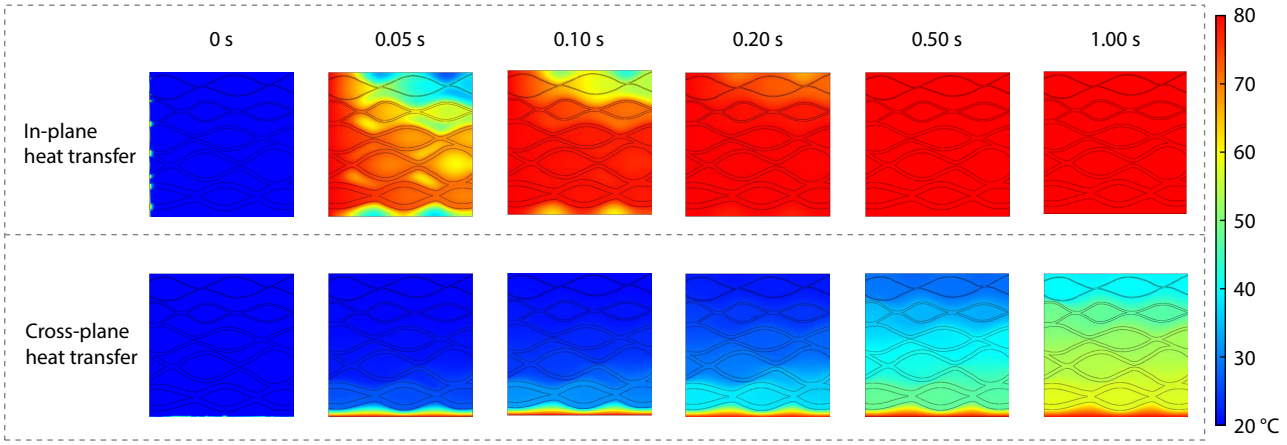

Fig. 7 In-plane and cross-plane heat-transfer behaviors simulated by the finite-element simulation.

fer process was significantly slower. High thermal conductivity allows the material to quickly conduct heat from the heating area to other parts, achieving a uniform temperature, which is essential for good Joule heating performance.[36,37] Fig. 6(b) shows the change in the surface temperature of the CNT-3/BN composites under different applied voltages. It can be seen that the surface temperature of the CNT-3/BN composite increases with increasing input voltage. When the input voltage is increased to 5 V, the surface temperature quickly reaches 81.3 °C and remains stable for a long time, indicating that its response time is fast, and it has sufficient heating stability and reliability. When the voltage is removed after heating for 400 s, the surface temperature of the composite film quickly drops to room temperature, indicating that the composite film has good heat dissipation performance. Moreover, as shown in Fig. 6(c), the surface temperature of the CNT-3/BN composite can be controlled by adjusting the step voltage, which once again confirms the rapid response characteristic of Joule heating of the composite. The relationship between the material surface temperature and input voltage was studied, as shown in Fig. 6(c). It can be seen that the surface saturation temperature of CNT-3/BN composite has a good linear relationship with U^2, which conforms to Joule's law.[38,39] Figs. 6(d) and 6(e) show infrared images of the CNT-3/BN composite under different input voltages. The thermal images show that the surface temperature is relatively homogeneous, with the highest temperature at the center and lower

https://doi.org/10.1007/s10118-025-3520-6

temperatures at the edge. A possible reason for this phenomenon is the fine thermal conductivity of the composite, which facilitates a rapid heat transfer at the edge. Furthermore, cyclic stability testing was performed on the sample, and the surface temperature remained nearly unchanged after ten heating-cooling cycles (Fig. 6f, Fig. S5 in ESI), indicating that the composite had excellent cyclic stability for practical applications. Generally, the prepared CNT/cellulose-BN/PVA composite with a gradient conductive and dual continuous structure achieves a relatively high EMI SE with enhanced *A*, fine thermal conductivity, and good Joual heating performance simultaneously, as summarized in Table S3 (in ESI). Therefore, the composite can be used as an EMI shielding material in extremely cold weather conditions.

Mechanical Property of the CNT/Cellulose-BN/PVA Composite

Fig. 8 shows the stress-strain curve and mechanical properties of CNT-3/BN. The stress-strain curve begins with a linear elastic region, showing a Young's modulus as high as 358.30 MPa. This is followed by plastic deformation and fracture, with the material exhibiting an average tensile strength of 12.93 MPa at a tensile strain of approximately 13%. The strain energy density up to fracture is calculated to be 98.13 $J \cdot m^{-3}$. Generally, the material demonstrates high strength and exceptional resistance to deformation, which meet the practical requirements for electronic devices. Finally, it must be noted that although we adopted the vertical impregnation-hot pressing method, it is generally considered a highly regarded technique for producing high-performance composites with well-controlled microstructures, high densities, and excellent mechanical properties. It should be recognized that this technique is better suited for the fabrication of small, flat, or simply curved high-performance materials, which can be integrated into larger, more complex structures by splicing, laminating, or embedding.

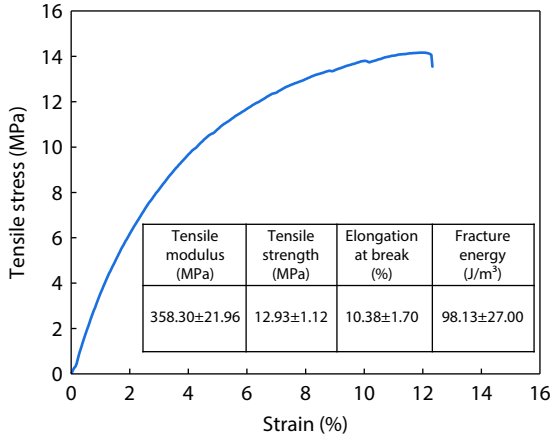

Fig. 8 Tensile stress–strain curve and mechanical parameters of CNT-3/BN.

CONCLUSIONS

In this work, a CNT/cellulose-BN/PVA composite with a gradient conductive structure and dual-continuous network structure was prepared by vertically impregnating CNT on a cellulose porous template, followed by BN/PVA impregnation-hot pressing molding. The gradient deposition of CNT on the porous cellulose template facilitates the construction of a gradient conductive network that endows the composite with an electrically conductive structure. The construction of the gradient structure enables an absorption-dominated EMI shielding mechanism and satisfies the EMI SE through the prolonged transmission path of the absorption-reflection-reabsorption process. Ultimately, a SE_T of 39.2 dB and *A* of 0.56 was achieved. The dual-continuous network structure can further improve the thermal conductivity for good Joule heating performance, which presents a Joule heating temperature of 81.3 °C. The present work offers a green and facile concept for designing multifunctional EMI-shielding cellulose composites, which can broaden the application of EMI shielding materials, especially under extreme weather conditions.

Conflict of Interests

The authors declare no interest conflict.

Electronic Supplementary Information

The electronic supplementary information (ESI) include the details of this work: formula for calculating the EMI SE of the CNT/cellulose-BN/PVA composites; detailed testing and calculation procedures for the laser flash thermal conductivity meter; SEM images of CNT and BN; thickness of CNT/cellulose-BN/PVA composites and weight contents of CNT and BN; the EMI SE of CNT/cellulose-BN/PVA composites in the frequency range of 8.2–12.4 GHz; permittivity and permeability measurements; relevant electromagnetic parameters of CNT/cellulose-BN/PVA composites; parameters of the finite element simulation models; finite element analysis model of CNT-3/BN; infrared images of CNT-3/BN composite material at 5 V for 10 cycles; comparison of EMI shielding, thermal conductivity, and Joule heating performance. ESI is available free ofcharge in the online version of this article at http://doi.org/10.1007/s10118-025-3520-6.

Data Availability Statement

Data supporting the findings of this study are available from the corresponding author upon reasonable request.

ACKNOWLEDGMENTS

This work was financially supported by the National Natural Science Foundation of China (No. 52103127) and the Opening Project of the State Key Laboratory of Polymer Materials Engineering (Sichuan University) (No. sklpme2022-4-10), and Shaanxi Provincial Science and Technology Department (No. 2025GH-YBXM-042).

REFERENCES

1 Jin, Y. S.; Wang, D. J.; Zhang, Y.; Liu, C. J.; Yan, L. P. A frequency selective surface absorber for electromagnetic shielding in enclosed cabins. *HPLPB* **2024**, *36*, 063002.

Graphical Abstract

Multifunctional CNT/cellulose-BN/PVA Composites Integrating Dual-continuous Network Structure with Gradient Conductivity for Electromagnetic Interference Shielding and Joule Heating

Xiao-Rui Wang, Ting-Ting Liu, Cheng-Hua Cui, Xin Xu, and Liang-Qing Zhang

Xi'an University of Science and Technology; Northwest Women's and Children's Hospital; Zhejiang University; Zhejiang Tongzheng Pipeline Technology Co., LTD.

An architecture featuring a gradient conductive network and three-dimensional dual-continuous network structure is constructed in carbon nanotubes/cellulose-boron nitride/poly(vinyl alcohol) (CNT/cellulose-BN/PVA) composite, which presents excellent electromagnetic interference shielding and recyclable Joule heating performance.

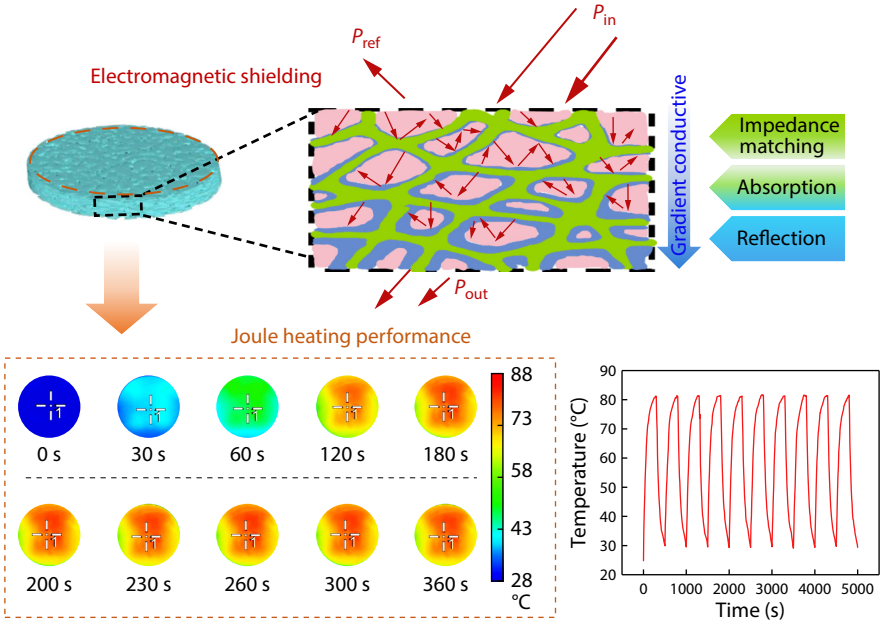

Chinese J. Polym. Sci. 2026, 44, 803–812 *https://doi.org/10.1007/s10118-025-3520-6*

2 Shahzad, F.; Alhabeb, M.; Hatter, C. B.; Anasori, B.; Soon, M. H.; Koo, C. M.; Gogotsi, Y. Electromagnetic interference shielding with 2D transition metal carbides (MXenes). *Science* **2016**, *353*, 1137–1140.
3 Xu, J. H.; Liu, T.; Zhang, Y. Z.; Zhang, Y. N.; Wu, K.; Lei, C. X.; Fu, Q.; Fu, J. J. Dragonfly wing-inspired architecture makes a stiff yet tough healable material. *Matter* **2021**, *4*, 2474–2489.
4 Ding, H. T.; Xia, Q. J.; Xu, Y. Research progress on electroless metal electromagnetic shielding fabric. *NCM.* **2022**, *50*, 11–14.
5 Cheng, J. Y.; Li, C. B.; Xiong, Y. F.; Zhang, H. B.; Raza, H.; Ullah, S.; Wu, J. Y.; Zheng, G. P.; Cao, Q.; Zhang, D. Q.; Zheng, Q. B.; Che, R. C. Recent advances in design strategies and multifunctionality of flexible electromagnetic interference shielding materials. *Nano-Micro Lett.* **2022**, *14*, 80.
6 Ding, H. T.; Wang, Y. T.; Luo, S. Q.; Xu, Y. The effect of fabric conductive grid structure on its electromagnetic shielding effectiveness. *NCM.* **2022**, *50*, 126–129.
7 Huo, Y. J.; Guo, D.; Yang, J. L.; Chang, Y. K.; Mu, C. P.; Nie, A.; Wang, B. C.; Xiang, J. Y.; Zhai, K.; Xue, T. Y.; Wen, F. S. Flexible graphene/bacterial celluloses janus structure film with excellent electromagnetic interference shielding and joule heating performance. *Mater. Chem. Phys.* **2022**, *287*, 126318.
8 Zhang, H. W.; Zheng, X. Y.; Jiang, R. J.; Liu, Z. H.; Li, W. Y.; Zhou, X. Research progress of functional composite electromagnetic shielding materials. *Eur. Polym. J.* **2023**, *185*, 111825.
9 Tian, K.; Hu, D. R.; Wei, Q.; Fu, Q.; Deng, H. Recent progress on multifunctional electromagnetic interference shielding polymer composites. *J. Mater. Sci. Technol.* **2023**, *134*, 106–131.
10 Hou, S. Y.; Ren, F.; Fu, B. Q. Research progress of graphene-based electromagnetic shielding composite. *NCM.* **2021**, *49*, 19–22.
11 Wang, Y. Q.; Zhao, W.; Tan, L. L.; Li, Y. R.; Qin, L.; Li, S. D. Review of polymer-based composites for electromagnetic shielding application. *Molecules* **2023**, *28*, 5628.
12 Zhang, Y. L.; Gu, J. W. A perspective for developing polymer-based electromagnetic interference shielding composites. *Nano-Micro Lett.* **2022**, *14*, 89.
13 Wang, L.; Ma, Z. L.; Zhang, Y. L.; Chen, L. X.; Cao, D. P.; Gu, J. W. Polymer-based EMI shielding composites with 3D conductive networks: a mini-review. *SusMat* **2021**, *1*, 413–431.
14 Li, J. C.; Zhao, X. Y.; Wu, W. J.; Ji, X. W.; Lu, Y. L.; Zhang, L. Q.

Bubble-templated rGO-graphene nanoplatelet foams encapsulated in silicon rubber for electromagnetic interference shielding and high thermal conductivity. *Chem. Eng. J.* **2021**, *415*, 129054.
15 Yasir, M.; Kim, S. R. 3D-structured polymer composites using advanced templating strategies for EMI shielding. *Polym. Compos.* **2025**, *46*, 9776-9821.
16 Guo, D. Y.; Tan, B. Z.; Jiang, X. J.; Gao, G. Y.; Lin, Y. Multifunctional polyimide/boron nitride nanosheet/$Ti_3C_2T_x$ MXene composite film with three-dimensional conductive network for integrated thermal conductive, electromagnetic interference shielding, and Joule heating performances. *Compos. Sci. Technol.* **2024**, *254*, 110690.
17 Lu, H. C.; Xia, Z. H.; Mi, Q. Y.; Zhang, J. M.; Zheng, X. J.; He, Z. Y.; Wu, J.; Zhang, J. Cellulose-based conductive films with superior joule heating performance, electromagnetic shielding efficiency, and high stability by in situ welding to construct a segregated MWCNT conductive network. *Ind. Eng. Chem. Res.* **2022**, *61*, 1773−1785.
18 Wang, Y. T.; Xin, Z. Y.; Shen, J. J.; Zhao, L. Y.; Wang, B. J.; Feng, X. L.; Mao, Z. P.; Sui, X. F. Acrylonitrile-butadiene-styrene-based composites derived from "fish-net"-inspired Pickering emulsion for high-performance electromagnetic interference shielding and thermal management. *Compos. Commun.* **2022**, *30*, 101085.
19 Zheng, S. F.; Wang, Y. Y.; Wang, X. S.; Lu, H. Research progress on high-performance electromagnetic interference shielding materials with well-organized multilayered structures. *Mater. Today Phys.* **2024**, *40*, 101330.
20 Jia, L.; Ding, X.; Sun, J.; Zhang, X.; Tian, X. Y. A controllable gradient structure of hydrophobic composite fabric constructed by silver nanowires and polyvinylidene fluoride microspheres for electromagnetic interference shielding with low reflection. *Compos. Part Appl. Sci. Manuf.* **2022**, *156*, 106884.
21 Luo, C. L.; Huang, M. L.; Sun, C.; Zhao, K. Y.; Guo, H.; Wang, M. Anisotropic electromagnetic wave shielding performance in Janus cellulose nanofiber composite films. *Mater. Today Phys.* **2024**, *44*, 101440.
22 Lei, Z. M.; Tian, D. K.; Liu, X. B.; Wei, J. H.; Rajavel, K.; Zhao, T.; Hu, Y. G.; Zhu, P. L.; Sun, R.; Wong, C. P. Electrically conductive gradient structure design of thermoplastic polyurethane composite foams for efficient electromagnetic interference shielding and ultra-low microwave reflectivity. *Chem. Eng. J.* **2021**, *424*, 130365.
23 Xu, Y. D.; Yang, Y. Q.; Yan, D. X.; Duan, H. J.; Zhao, G. Z.; Liu, Y. Q. Gradient structure design of flexible waterborne polyurethane conductive films for ultraefficient electromagnetic shielding with low reflection characteristic. *ACS Appl. Mater. Interfaces* **2018**, *10*, 19143−19152.
24 Hou, M. H.; Feng, Y. J.; Yang, S. Q.; Wang, J. Multi-hierarchically structural polycaprolactone composites with tunable electromagnetic gradients for absorption-dominated electromagnetic interference shielding. *Langmuir* **2023**, *39*, 6038−6050.
25 Peng, Q.; Ma, M.; Chen, S.; Shi, Y. Q.; He, H. W.; Wang, X. Magnetic-conductive bi-gradient structure design of CP/PGFF/Fe_3O_4 composites for highly absorbed EMI shielding and balanced mechanical strength. *J. Mater. Sci. Technol.* **2023**, *133*, 102−110.
26 Liang, C. B.; Ruan, K. P.; Zhang, Y. L.; Gu, J. W. Multifunctional flexible electromagnetic interference shielding silver nanowires/cellulose films with excellent thermal management and joule heating performances. *ACS Appl. Mater. Interfaces* **2020**, *12*, 18023−18031.
27 Zhang, L. Q.; Zhou, F.; Shi, Q.; Zhang, Z. Y.; Yang, S. G.; Yan, D. X.; Peng, L. G.; Zhai, X. W. Multifunctional cellulose composite films with dual-continuous CNT/BN networks for synchronously enhanced electromagnetic interference shielding ability and thermal conductivity. *Cellulose* **2024**, *31*, 2397−2412.
28 Wang, Y. F.; Chen, R.; Wen, F. Y.; Bai, Y. G.; He, Y. S.; Cheng, L.; Tan, H. Y.; Ma, J. R.; Lian, P. B.; Gu, Y. X.; Mu, J. X. Developing PEEK composites with exceptional thermal conductivity and electromagnetic shielding properties by constructing a dense dual-continuous filler network. *Colloid Surf. A-Physicochem. Eng. Asp.* **2024**, *702*, 135021.
29 Cui, J. M.; Yang, S. G.; Zhang, R. B.; Cao, Y.; Wang, Y. B.; Zeng, X. B.; Liu, F.; Ungar, G. Continuous spectrum of morphologies and phase behavior across the contact zone from poly(l-lactide) to poly(d-lactide): stereocomplex, homocrystal, and between. *Macromolecules* **2023**, *56*, 8754−8766.
30 Lyu, B.; Wang, Y. C.; Gao, D. G.; Guo, S. H.; Zhou, Y. Y.; Ma, J. Z. Ultra-low reflection electromagnetic interference shielding nanofiber film with effective solar harvesting and self-cleaning. *Collagen and Leather* **2024**, *6*, 2.
31 Xue, T. T.; Yang, Y.; Yu, D. Y.; Wali, Q.; Wang, Z. Y.; Cao, X. S.; Fan, W.; Liu, T. X. 3D printed integrated gradient-conductive MXene/CNT/polyimide aerogel frames for electromagnetic interference shielding with ultra-low reflection. *Nano-Micro Lett.* **2023**, *15*, 45.
32 Lv, H. L.; Yang, Z. H.; Pan, H. G.; Wu, R. B. Electromagnetic absorption materials: Current progress and new frontiers. *Prog. Mater. Sci.* **2022**, *127*, 100946.
33 Chen, P.; He, S. B.; Wang, T. Y.; Wang, C. C.; Tao, J. R.; Li, Y. W. Melanin-like nanofibers with highly ordered structures achieve ultrahigh specific electromagnetic interference shielding efficiency. *Nat. Commun.* **2025**, *16*, 7127.
34 Wang, M.; Tang, X. H.; Cai, J. H.; Wu, H.; Shen, J. B.; Guo, S. Y. Construction, mechanism and prospective of conductive polymer composites with multiple interfaces for electromagnetic interference shielding: a review. *Carbon* **2021**, *177*, 377−402.
35 Huang, M. L.; Luo, C. L.; Sun, C.; Zhao, K. Y.; Wang, M. In-situ microfibrilization of liquid metal droplets in polymer matrix for enhancing electromagnetic interference shielding and thermal conductivity. *Compos. Sci. Technol.* **2024**, *255*, 110724.
36 Zhou, B.; Zhang, Z.; Li, Y. L.; Han, G. J.; Feng, Y. Z.; Wang, B.; Zhang, D. B.; Ma, J. M.; Liu, C. T. Flexible, robust, and multifunctional electromagnetic interference shielding film with alternating cellulose nanofiber and MXene layers. *ACS Appl. Mater. Interfaces* **2020**, *12*, 4895−4905.
37 Ren, F.; Zhang, J. L.; Wu, T.; Zhang, F. D.; Guo, Z. Z.; Jin, Y. L.; Ren, P. G. Bioinspired, ultra-light and sandwich structured MXene–AgNWs/cellulose nanofiber porous film for excellent electromagnetic interference shielding with Joule heating performance. *Cellulose* **2024**, *31*, 2341−2353.
38 Zhao, X.; Wang, L. Y.; Tang, C. Y.; Zha, X. J.; Liu, Y.; Su, B. H.; Ke, K.; Bao, R. Y.; Yang, M. B.; Yang, W. Smart $Ti_3C_2T_x$ MXene fabric with fast humidity response and joule heating for healthcare and medical therapy applications. *ACS Nano* **2020**, *14*, 8793−8805.
39 Cheng, Y.; Cui, G.; Liu, C. H.; Liu, Z. T.; Yan, L. G.; Liu, B. Y.; Yuan, H.; Shi, P. C.; Jiang, J.; Huang, K. W.; Wang, K.; Cheng, S. T.; Li, J. L.; Gao, P.; Zhang, X. F.; Qi, Y.; Liu, Z. F. Electric current aligning component units during graphene fiber joule heating. *Adv. Funct. Mater.* **2022**, *32*, 2103493.